Available online at www.sciencedirect.com
ScienceDirect
Journal of Nuclear Materials 367–370 (2007) 468–472
journal of nuclear materials
www.elsevier.com/locate/jnucmat

Behavior of helium in steel 16Cr12W2VTaB under various implantation temperatures

I.I. Chernov [a], S.Yu. Binyukova [a], B.A. Kalin [a,*], Myo Htet Win [a], Than Swe [a], S.V. Chubarov [a], A.N. Kalashnikov [a], A.G. Ioltukhovskiy [b], M.V. Leontyeva-Smirnova [b]

[a] *Moscow Engineering Physics Institute (State University), 31 Kashirskoye sh., Moscow 115409, Russia*
[b] *A.A. Bochvar Institute of Inorganic Materials (SSC RF-VNIINM), P.O. Box 369, Moscow 123060, Russia*

Abstract

Gaseous porosity formation and helium behavior have been investigated in the reduced activation ferritic–martensitic steel 16Cr12W2VTaB irradiated with 40 keV He^+ ions up to a fluence of 5×10^{20} m^{-2} at temperatures from 290 to 900 K in two initial conditions: normalized + tempered (HT-1), and cold rolled + annealed (HT-2). After HT-1, cavitation was observed above 770 K, where bubbles with a maximum diameter 1 nm were formed. Large bubbles with a mean diameter 8 nm formed when irradiated at 900 K. On the other hand, a high density of small bubbles formed at the lower irradiation temperature of 570 K after HT-2. At 900 K, bubbles had an extremely nonuniform distribution in size, depending on their locations. The helium thermodesorption spectra had two intensive peaks owing to polymorphic transformation during heating. The peaks widened and gas release began at higher temperatures with formation of large bubbles.

1. Introduction

The creation of heat and radiation resistant steels and alloys characterized by reduced long-term activation, including ferritic–martensitic steels of the 12% Cr type, is a new materials development trend for structural applications in the field of nuclear technologies. Among them, a new 16Cr12W2VTaB type ferritic–martensitic steel has been recently created for potential use in components of both the first wall and blanket of a DEMO reactor and the ITER test module, as well as for use as a structural material for the active zone of breeder power reactors [1]. However, the behavior of 12% Cr type chromium steels has not yet been well enough studied in conditions of accumulation and/or implantation (in fusion reactors) of considerable concentrations of gaseous atoms, including helium.

The purpose of this work is to clarify the gaseous porosity formation and helium behavior peculiarities in ferritic–martensitic steel 16Cr12W2VTaB irradiated with He^+ ions, with a special concern on the initial condition of the material, so as to obtain information on the influence of a large amount of helium.

* Corresponding author. Tel.: +7 095 323 9267; fax: +7 095 324 3165.
E-mail addresses: Kalin@mephi.ru, BAKalin@mephi.ru (B.A. Kalin).

0022-3115/$ - see front matter © 2007 Elsevier B.V. All rights reserved.
doi:10.1016/j.jnucmat.2007.03.115

2. Experimental procedure

The chemical composition of steel was presented in [1]. Two types of pre-irradiation heat treatments were used for the steel: (1) normalizing at 1370 K/40 min followed by air cooling + tempering at 990 K/3 h, air cooling (HT-1); (2) cold rolling + annealing at 1070–1080 K/1 h, air cooling (HT-2). The samples were irradiated in ion accelerator ILU-3 [2] with 40 keV He^+ ions up to a fluence of 5×10^{20} m^{-2} at ion flux about 10^{18} $He^+/(m^2\ s)$ in the temperature range of 270–900 K. The microstructure of samples thinned from the unirradiated side was investigated in TEM, JEM-2000EX. Helium release was studied by helium thermodesorption spectrometry (HTDS) for two rates of heating $\alpha = 1.2$ and 3 K/s, using a helium partial pressure meter (sensitivity: 10^8–10^{10} at He/s). The effective activation energies of helium release E^{eff} for the HTDS peaks were calculated by the 'tempering' method [3,4].

3. Results and discussion

3.1. TEM observations

After HT-1, the structure of steel 16Cr12W2VTaB looked like plate-type sorbite (Fig. 1). The rolling structure partly remained after HT-2, i.e. defects caused by rolling were not totally annealed-out. In addition, the existence of twins proved by the presence of satellite spots near the matrix reflections. The observed streaks on the electron diffraction picture (long windedness of reciprocal lattice nodes) and additional spots (Fig. 2) would testify that the twin plates are very narrow and there is some elastic deformation at twin boundaries [5].

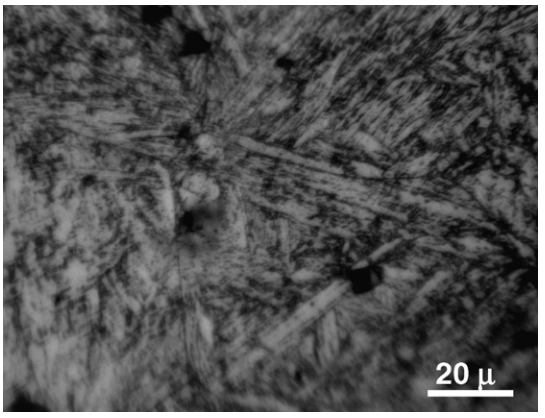

Fig. 1. Initial structure of steel 16Cr12W2VTaB after HT-1 (optical micrograph).

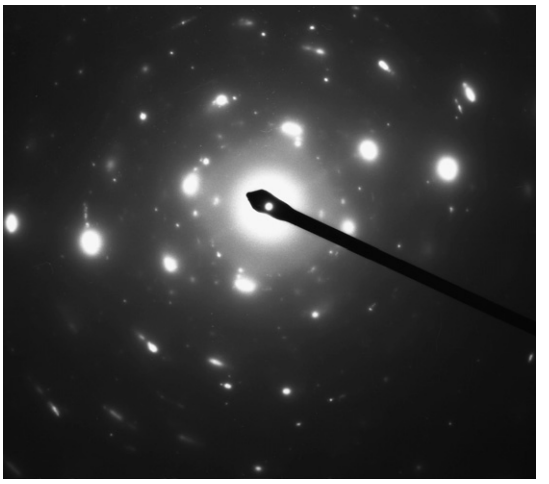

Fig. 2. Electron diffraction picture from steel structure after HT-2.

The typical TEM photographs of steel 16Cr12W2VTaB irradiated with He^+ ions after HT-1 and HT-2 are shown in Figs. 3 and 4, respectively. Table 1 summarizes the bubble parameters in the steel irradiated in these two initial states.

As can be seen from Table 1, bubbles were not formed in samples irradiated at 290 and 570 K after HT-1. Only defect loop and dislocation structures were observed. Helium should be in the lattice in the form of various helium-vacancy or other type complexes [4,6,7]. Bubbles were also not explicitly found in samples irradiated at 690 K, though the presence of definite characteristic contrast in the condition of de-focusing of TEM image [8] implied

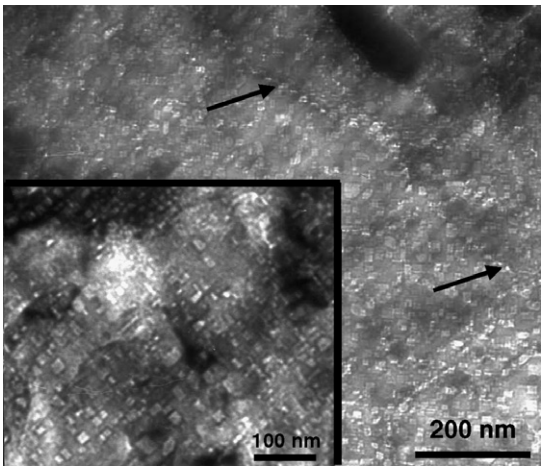

Fig. 3. Typical microstructure of sample irradiated at 900 K after HT-1.

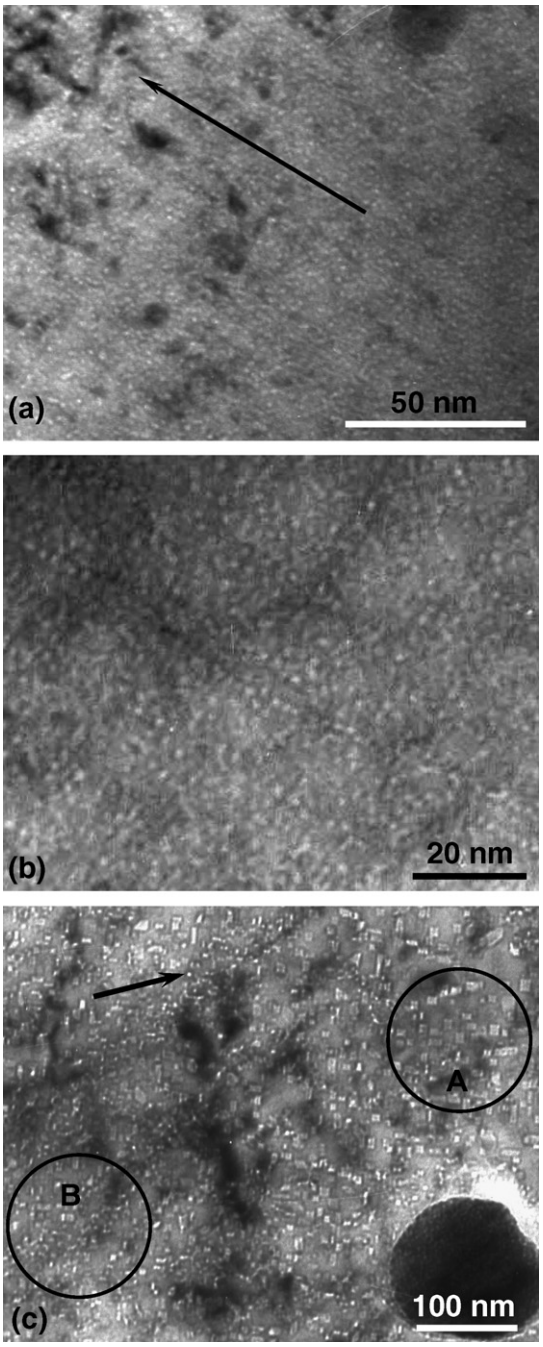

Fig. 4. Typical microstructure of samples irradiated at 570 K (a), (b) and 900 K (c) after HT-2.

possible presence of fine bubbles with sizes corresponding to the resolution limit of TEM. Bubbles were well-observed by TEM only at above 770 K for this heat treatment. The size of bubbles sharply increased and their density decreased by three orders of magnitude with increase of radiation temperature up to 900 K. The characteristic feature of these bubbles was their faceting and non-uniform distribution in the matrix: along with large faceted bubbles there were local zones with fine spherical bubbles of high density. The large bubbles were predominantly located on dislocations (shown by arrows in Fig. 3). The estimation made using the procedure formerly presented [9] shows that the faceted bubbles formed at 900 K should be pre-equilibrium (i.e., $p < 2\gamma/r$, where p is helium pressure, γ the surface tension and r bubble radius) and the bubbles obtained at other temperatures should be overpressured.

The size distribution of helium bubbles in samples irradiated after HT-1 at temperatures other than 900 K was close to that of Gaussian and the most probable size of the bubbles and their mean diameter were practically agreed with each other.

Along with the defect loop structure, a high density of the smallest bubbles was observed in samples irradiated at the temperature of 570 K after HT-2. These bubbles had a tendency to be predominantly located along the rolling direction in the matrix (shown by arrow in Fig. 4(a)). Chains of larger bubbles were observed at twin boundaries (Fig. 4(b)). The bubble sizes grew and their density slightly decreased with increasing irradiation temperature up to 770 K (see Table 1). The bubbles were aligned in [0 2 0] and [2 1 0] directions. The increase of irradiation temperature up to 900 K gave a rise in the degree of porosity. At that temperature, the density of bubbles decreased nearly by an order of magnitude in comparison with that obtained at 770 K. For the maximum irradiation temperature, the dispersion of bubbles in samples and their size distribution in grains were extremely non-uniform (Fig. 4(c)). Along with large cavities (area A), zones with small bubbles of a high density were observed (area B), as well as long interlayers with fine bubbles located between zones of large bubbles (shown by arrow in Fig. 4(c)). This resulted in a double-humped histogram.

Although bubble evolution started at higher temperature after HT-1 than after HT-2, a greater number of coarse pores were formed and greater gaseous swelling of the irradiated layer was observed after HT-1 following high temperature He^+ irradiation (900 K).

3.2. The results of HTDS

In contrast to austenitic steels having only one main HTDS peak [10], thermodesorption spectra

Table 1
Bubble parameters for steel 16Cr12W2VTaB irradiated with He^+ ions at different temperatures (d_{max} and $\bar{d}$ are the maximum and mean bubble diameters, respectively; ρ is the bubble number density; and S is the gaseous swelling of an irradiated layer)

Heat treatment	T_{irrad}, K	d_{max}, nm	$\bar{d}$, nm	ρ[a], m^{-3}	S[a], %
HT-1	290	–	–	–	–
	570	–	–	–	–
	690	–(?)	–(?)	–(?)	–(?)
	770	~1.5	~0.6	$\sim 10^{25}$	~0.03
	900	~20	7.5	$(2.9 \pm 0.6) \cdot 10^{22}$	1.3 ± 0.3
HT-2	270	–	–	–	–
	570	~2	0.8	$(2.1 \pm 0.5) \times 10^{24}$	0.07 ± 0.02
	690	~4	1.2	$(1.6 \pm 0.4) \times 10^{24}$	0.18 ± 0.05
	770	~7	1.8	$(7.1 \pm 1.8) \times 10^{23}$	0.37 ± 0.09
	900	~17	4.8	$(5.9 \pm 1.4) \times 10^{22}$	0.8 ± 0.2

[a] Scatter of data was determined by accuracy of foil thickness measurement in TEM.

for steel 16Cr12W2VTaB had two intensive peaks (Fig. 5) owing to polymorphic $\alpha \rightarrow \gamma$ transformation during heating as for Fe–9Cr ferritic alloy [11] and other ferritic–martensitic steels [12]. The first peak was conditioned by bubble migration to the specimen surface from ferrite matrix and the second one by that from austenite. The gas release temperature range depended on the irradiation temperature, the initial structural state of the steel and the heating rate. The HTDS peaks became widened and shifted to higher temperatures in case that bubbles were formed during irradiation (Table 1, Fig. 6). This trend was intensified for larger bubbles since the migration of large bubbles should be more strongly impeded as compared to small bubbles [13].

Differences in the HTDS spectra between two different heat treatments are the followings: gas release was initiated at a lower temperature and peak temperatures were lower for HT-1 than those for HT-2 for irradiation temperatures less than 690 K. On the contrary, gas release started later and the main peak temperatures were higher for samples irradiated at high temperatures for the HT-1 condition (Fig. 6). The increase of heating rate shifted the HTDS peaks to a higher temperature range. This allows calculating the effective activation energy of helium desorption. For example, $E^{eff} = (4.0 \pm 0.8)$ eV was obtained for the second peak of the steel irradiated at 770 K after HT-2. This value would testify to a dominant contribution of volume diffusion on bubble migration mechanism in austenite [4,14].

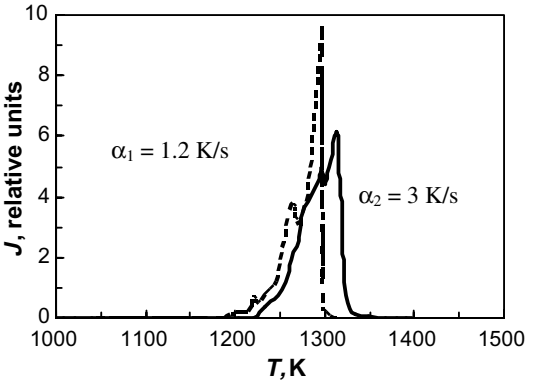

Fig. 5. HTDS spectra of samples irradiated at 770 K after HT-2 for two different constant heating rates, α.

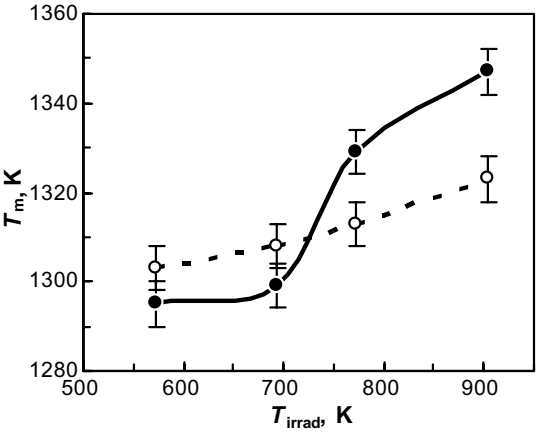

Fig. 6. HTDS main peak temperature vs. helium-ion implantation temperature of samples irradiated after HT-1 (●) and HT-2 (○) for $\alpha = 3$ K/s.

4. Summary

The pre-irradiation microstructure of steel 16Cr12W2VTaB significantly influenced the gas bubble evolution character and the helium behavior

after helium implantation. Bubbles did not form and defect loop structure was observed at irradiation temperatures of 290–570 K. Bubbles were formed only above 770 K for HT-1. Meanwhile, for HT-2, bubble evolution was noticed even at lower temperature of 570 K. However, for high-temperature irradiation (900 K), both bubble size and gaseous swelling were smaller than those for HT-1. At irradiation temperatures up to 690 K gas release was initiated at lower temperatures and peak temperatures were lower for HT-1 than those for HT-2 under HTDS measurements and the release of gas conversely started later and the main peak temperatures were higher for samples irradiated at high-temperatures in the HT-1 condition. The HTDS spectra for steel 16Cr12W2VTaB had two intensive peaks owing to polymorphic transformation during heating. Volume diffusion would dominate bubbles migration during the gas release.

References

[1] A.G. Ioltukhovskiy, M.V. Leontyeva-Smirnova, M.I. Solonin, et al., J. Nucl. Mater 307–311 (2002) 532.
[2] V.M. Gusev, N.P. Busharov, S.M. Naftulin, et al., Equipments and Experiment Technique 4 (1969) 19 (in Russian).
[3] V.F. Zelenskij, I.M. Nekludov, V.V. Ruzhitskij, et al., J. Nucl. Mater. 151 (1987) 22.
[4] B.A. Kalin, I.I. Chernov, A.N. Kalashnikov, M.N. Esaulov, Problems of Atomic Sci. Ser.: Radiat. Damage Phys. Radiat. Mater. Sci. 1(65)/2(66) (1997) 53 (in Russian).
[5] P.B. Hirsch, A. Howie, R.B. Nicholson, D.W. Pashley, M.J. Whelan, Electron Microscopy of Thin Crystals, Butterworths, London, 1965.
[6] S.E. Donnelly, Radiat. Eff. 90 (1985) 1.
[7] I.I. Chernov, B.A. Kalin, A.N. Kalashnikov, V.M. Ananin, J. Nucl. Mater. 271&272 (1999) 333.
[8] J.W. Edington, Practical Electron Microscopy in Materials Science. Part 4: Typical Electron Microscope Investigations, Macmillan, London, 1976.
[9] S.Yu. Binyukova, I.I. Chernov, B.A. Kalin, Than Swe, J. Nucl. Mater., these Proceedings, doi:10.1016/j.jnucmat.2007.03.110.
[10] G.D. Tolstolutskaya, V.V. Ruzhitsky, I.E. Kopanets, S.A. Karpov, V.V. Bryk, V.N. Voevodin, Problems of Atomic Sci. Ser.: Radiat. Damage Phys. Radiat. Mater. Sci. 3 (2004) 3 (in Russian).
[11] K. Ono, K. Arakawa, H. Shibasaki, et al., J. Nucl. Mater. 329–333 (1987) 933.
[12] S.Yu. Binyukova, I.I. Chernov, Myo Htet Vin et al., in: Proceedings of the 16th International Conference on Radiat. Physics of Solids, Sevastopol, Ukraine, July 3–8, 2006, p. 253.
[13] K. Ono, H. Trinkaus, K. Arakawa, K. Hojou, J. Nucl. Mater. 307–311 (2002) 1507.
[14] A.G. Zaluzhnij, Yu.N. Sokurskij, V.V. Tebus, Helium in Reactor Materials, Energoatomizdat, Moscow, 1988.